

The effect of primordial black holes on 21cm fluctuations

Hiroyuki Tashiro¹ and Naoshi Sugiyama^{2,3}

¹*Physics Department, Arizona State University, Tempe, AZ 85287, USA*

²*Department of Physics and Astrophysics & Kobayashi-Maskawa Institute for the Origin of Particles and the Universe, Nagoya University, Chikusa, Nagoya 464-8602, Japan*

³*Institute for the Physics and Mathematics of the Universe (IPMU), The University of Tokyo, Kashiwa, Chiba, 277-8568, Japan*

6 November 2018

ABSTRACT

The 21 cm signal produced by non-evaporating primordial black holes (PBHs) is investigated. X-ray photons emitted by accretion of matter onto a PBH ionize and heat the intergalactic medium (IGM) gas near the PBH. Using a simple analytic model, we show that this X-ray heating can produce an observable differential 21 cm brightness temperature. The region of the observable 21 cm brightness temperature can extend to 1–10 Mpc comoving distance from a PBH depending on the PBH mass. The angular power spectrum of 21 cm fluctuations due to PBHs is also calculated. The peak position of the angular spectrum depends on PBH mass, while the amplitude is independent of PBH mass. Comparing this angular power spectrum with the angular power spectrum caused by primordial density fluctuations, it is found that both of them become comparable if $\Omega_{\text{PBH}} = 10^{-11}(M/10^3 M_{\odot})^{-0.2}$ at $z = 30$ and $10^{-12}(M/10^3 M_{\odot})^{-0.2}$ at $z = 20$ for the PBH mass from $10 M_{\odot}$ to $10^8 M_{\odot}$. Finally we find that the Square Kilometer Array can detect the signal due to PBHs up to $\Omega_{\text{PBH}} = 10^{-5}(M/10^3 M_{\odot})^{-0.2}$ at $z = 30$ and $10^{-7}(M/10^3 M_{\odot})^{-0.2}$ at $z = 20$ for PBHs with mass from $10^2 M_{\odot}$ to $10^8 M_{\odot}$.

Key words: cosmology: theory – large-scale structure of universe

1 INTRODUCTION

primordial black holes (PBHs) could have formed in the early Universe (Carr & Hawking 1974; Carr 1975). Although there is no direct evidence of their existence of PBHs, PBHs are attracting attention as a way of constraining physics in the early Universe. In particular, one of the main generation mechanisms of PBHs is the gravitational collapse of an overdense region at the horizon scale when the amplitude of the overdensity exceeds a critical threshold. Therefore the resultant mass function and the abundance of PBHs depend on the amplitude of primordial density fluctuations at the horizon-crossing epoch (Green et al. 2004). The PBH abundance is expected to be a probe of primordial density fluctuations on small scales, which cannot be accessed by Cosmic Microwave Background or large-scale-structure observations.

Constraints on the abundance of PBHs have been extensively studied and continue to be updated (Carr et al. 2010). PBHs with mass less than 10^{15} g have evaporated by the present epoch because the evaporation time scale by Hawking radiation is less than the Hubble time scale today (Hawking 1974). However evaporation of PBHs generates additional entropy in the Universe after inflation (Zel'dovich & Starobinskii 1976), affects big bang nucleosynthesis (Vainer et al. 1978; Vainer & Naselskii 1978; Miyama & Sato 1978; Zeldovich et al. 1977; Lindley 1980) and distorts the CMB blackbody spectrum (Tashiro & Sugiyama 2008). PBH evaporation may also produce the observable gamma-ray background (Page & Hawking 1976; MacGibbon & Carr 1991). According to measurements of these cosmological phenomena, there are strong constraints on the abundance of PBHs with mass less than 10^{15} g.

PBHs with mass larger than 10^{15} g survive in the present Universe. One of the constraints on such PBHs can be set from the fact that the current density parameter of PBHs, Ω_{PBH} , cannot exceed the cold dark matter density parameter observed at the present epoch, Ω_{C} . Conventionally, the constraint on PBH abundance is given by $\beta(M)$ which is the fraction of regions of mass M collapsing into PBHs at the formation epoch (Carr 1975). The constraint on the density parameter of PBHs today, $\Omega_{\text{PBH}} < \Omega_{\text{C}}$, implies $\beta < 2 \times 10^{-18}(M/10^{15}\text{g})^{1/2}$ from WMAP 7-year data, i.e., $\Omega_{\text{C}} = 0.22$ (Komatsu et al.

2011). Microlensing observations also constrain the abundance of non-evaporating PBHs (Alcock et al. 2001). Ricotti et al. (2008) have obtained the constraint on PBHs with mass larger than $0.1 M_{\odot}$, by investigating the effects of such PBHs on cosmic reionization and CMB temperature anisotropies. Future gravitational wave observations are also expected to provide a probe of the massive PBH abundance (Ioka et al. 1999; Inoue & Tanaka 2003).

In this paper, we evaluate the 21 cm brightness temperature produced by PBHs and study the potential of 21 cm observations to give a constraint on the abundance of PBHs. Mack & Wesley (2008) have investigated the signatures of evaporating PBHs in 21 cm brightness temperature. Accordingly, they have concentrated on PBHs whose mass range is $5 \times 10^{13} \text{ g} \lesssim M_{\text{PBH}} \lesssim 10^{17} \text{ g}$. On the contrary, here, we focus on non-evaporating PBHs with mass much larger than 10^{15} g . After the epoch of matter-radiation equality, gas and matter can accrete onto PBHs. It has been shown that PBHs with large mass could produce X-ray and UV photons through the accretion of matter onto PBHs and these photons heat up and ionize intergalactic medium (IGM) (Carr 1981; Gnedin et al. 1995; Miller & Ostriker 2001; Ricotti et al. 2008). Therefore, the heated and ionized IGM gas may produce an observable deviation of the 21 cm brightness temperature from the background even before the birth of the first stars and galaxies ($z > 30$). Our aim in this paper is to evaluate this deviation and to discuss the potential of 21 cm observations to constrain the non-evaporating PBH abundance.

The paper is organized as follows. In section 2, using a simple model of X-ray photon flux due to the accretion onto a PBH, we evaluate the ionization and temperature profile near a PBH. In section 3, we calculate the spin temperature and the brightness temperature induced by a PBH. In section 4, the angular power spectrum of 21 cm fluctuations due to PBHs are evaluated. Section 5 is devoted to the conclusion. Throughout this paper, we use parameters for a flat Λ CDM model: $h = 0.7$ ($H_0 = h \times 100 \text{ km/s/Mpc}$), $\Omega_{\text{B}} = 0.05$ and $\Omega_{\text{M}} = 0.26$. These parameters are consistent with WMAP results (Komatsu et al. 2011).

2 IONIZATION AND HEATING OF IGM BY A PBH

After the epoch of matter-radiation equality, matter can accrete onto a non-evaporating PBH, whose mass is larger than 10^{15} g . Therefore, the accretion disk of a non-evaporating PBH can be a source of X-ray photons before first stars and galaxies form ($z > 30$). For example, the non-evaporating PBHs are one of the candidates for super massive black hole seeds. PBHs whose masses exceed $10^5 M_{\odot}$ cannot be directly formed through gravitational collapse since the time scale of the collapse becomes longer than cosmological time. Accordingly only the accretion after the formation, which induces X-ray photon emission, makes possible to form such massive black holes (Düchting 2004; Khlopov et al. 2005). It is difficult to theoretically predict the accurate X-ray photon spectrum from PBHs, because the X-ray spectrum depends on the detailed condition of the accretion and the environment of PBHs such as the amount of neutral hydrogen. Hence, for simplicity, we assume that the PBH accretion powers a miniquasar with a power-law spectrum of X-ray photons, according to Kuhlen & Madau (2005),

$$F(E) = \mathcal{A} E^{-1} \text{ s}^{-1}, \quad (1)$$

where \mathcal{A} is set to correspond to the tenth of the Eddington luminosity. Here we consider the range of the photon energy E from 200 eV to 100 keV since we assume that emitted photons whose energy are lower than 200 eV are immediately absorbed by the surrounding gas of the PBH. Following Zaroubi et al. (2007), we evaluate the ionization and heating of IGM due to massive PBHs in this section.

The number density of photons per unit time per unit area at distance r from the source is given by

$$\mathcal{N}(E; r) = e^{-\tau(E; r)} \frac{\mathcal{A}}{(4\pi r^2)} E^{-1} \text{ cm}^{-2} \text{ s}^{-1}, \quad (2)$$

$$\tau(E; r) = \int_0^r n_{\text{H}} x_{\text{H}} \sigma(E) dr, \quad (3)$$

where x_{H} is the hydrogen neutral fraction, n_{H} is the mean number density of hydrogen at a redshift z and $\sigma(E)$ is the absorption cross-section per hydrogen atom. In order to take into account the contribution from helium atoms as well as hydrogen atoms, we adopt the fitting formula by Zdziarski & Svensson (1989),

$$\sigma = 4.25 \times 10^{-21} \left(\frac{E}{250 \text{ eV}} \right)^{-p} \text{ cm}^2, \quad p = \begin{cases} 2.65 & \text{for } E < 250 \text{ eV,} \\ 3.30 & \text{for } E > 250 \text{ eV.} \end{cases} \quad (4)$$

Using the function $\mathcal{N}(E; r)$, we can write the ionization rate per hydrogen atom at the distance r from the source as

$$\Gamma(r) = \int_{E_0}^{\infty} \sigma(E) \mathcal{N}(E; r) \left(1 + \frac{E}{E_0} \phi(E, x_e) \right) \frac{dE}{E}, \quad (5)$$

where the term, $(E/E_0)\phi(E, x_e)$, is introduced to consider the secondary ionization due to the photoelectrons produced by energetic photons ($E > 100 \text{ eV}$). We apply the fitting formula of ϕ by Dijkstra et al. (2004) for the low energy region $E < 0.5 \text{ keV}$ and by Shull & van Steenberg (1985) for the high energy region $E > 0.5 \text{ keV}$.

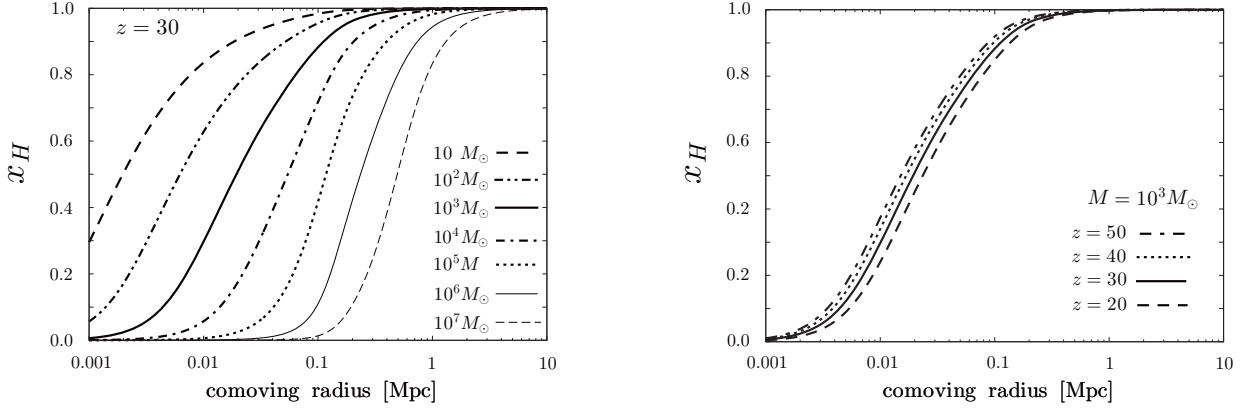


Figure 1. The neutral fraction of hydrogen as a function of comoving distance from the source. The left panel shows the dependence on mass at $z = 30$. The lines represent the neutral fraction with masses ranging from $10 M_{\odot}$ to $10^7 M_{\odot}$ from left to right. The right panel shows the dependence on the redshift for a PBH with $M = 10^3 M_{\odot}$. The dotted-dashed, dotted, solid and dashed lines represent the neutral fraction at $z = 50$, $z = 40$, $z = 30$ and $z = 20$, respectively.

The neutral fraction of hydrogen is obtained by solving the equation of the ionization-recombination equilibrium

$$\alpha_H n_H^2 (1 - x_H)^2 = \Gamma(r) n_H x_H, \quad (6)$$

where α_H is the recombination cross-section; $\alpha_H = 2.6 \times 10^{-13} \text{cm}^3 \text{s}^{-1}$,

Solving Eq. (6), we show the neutral fraction of hydrogen for different masses and for different redshifts in the left and right panels of Fig. 1, respectively. Here we assume that the density around a PBH is the same as the mean density of the Universe. The comoving radius of the ionization sphere is made large by a massive PBH. Increasing the mass of the PBH means increasing the number of the ionization photons, because we assume that the flux of the ionization photons is proportional to a tenth of the Eddington luminosity. As the Universe evolves, the comoving radius of the ionization sphere increases slowly.

Next, we evaluate the kinetic temperature of the IGM around a PBH. The heating rate per unit volume per unit time at a distance r from the source is obtained by considering the photons absorbed by the IGM at r ,

$$\mathcal{H}(r) = f n_H x_H(r) \int_{E_0}^{\infty} \sigma(E) \mathcal{N}(E; r) dE, \quad (7)$$

where f is the fraction of the photon energy absorbed through the collisional excitations of the IGM. Shull & van Steenberg (1985) provided a simple fitting formula $f = C [1 - (1 - x^a)^b]$, where $C = 0.9771$, $a = 0.2663$, $b = 1.3163$ and x is the ionized fraction $x = 1 - x_H$.

The kinetic temperature of the IGM at a distance r , $T_k(r)$, is determined by the balance between the heating and the Compton cooling due to CMB photons,

$$\mathcal{H}(r) = \frac{8\sigma_T}{3m_e} T_{\gamma}^4 (1 - x_H) (T_k(r) - T_{\gamma}) + 2HT_k(r), \quad (8)$$

where σ_T is the cross section for the Compton scattering and T_{γ} is CMB temperature. Here we also take into account the cooling by the expansion of the Universe.

Fig. 2 shows the IGM kinetic temperature profiles for different masses in the left panel and for different redshifts in the right panel. Here we add the background kinetic temperature to the kinetic temperature in order to match both temperatures at a large distance from a PBH. Near the source, the temperature is determined by the heating rate and the Compton cooling rate. With increasing the distance from the source, the neutral fraction grows and the optical depth τ becomes larger. Accordingly, the number density of photons damps as shown in Eq. (2). As a result, the temperature starts to decrease rapidly. Because the Compton cooling depends on the number of free electrons, this cooling becomes ineffective at a distance where the neutral fraction of hydrogen becomes almost unity. For example, this scale corresponds to 0.1 comoving Mpc for a PBH with $M = 10^3 M_{\odot}$ at $z = 30$. Beyond this point, the temperature mildly decreases due to the cooling of the cosmic expansion. The kinetic temperature at the inner side is independent on a PBH mass. However the region of the high temperature becomes larger as the PBH mass increases. In the right panel of Fig. 2, the redshift dependence of the kinetic temperature is shown. The larger the neutral hydrogen density is, the larger the heating efficiency becomes as in Eq. (7). Therefore the temperature becomes high as the redshift increases.

In this section, we obtained the neutral fraction of hydrogen by solving the equation of the ionization-recombination equilibrium, Eq. (6). However the recombination time scale is much smaller than the ionization time scale at the redshifts we are interested in. Therefore Eq. (6) might be incorrect. In this limit, we can neglect the recombination effect. Without the

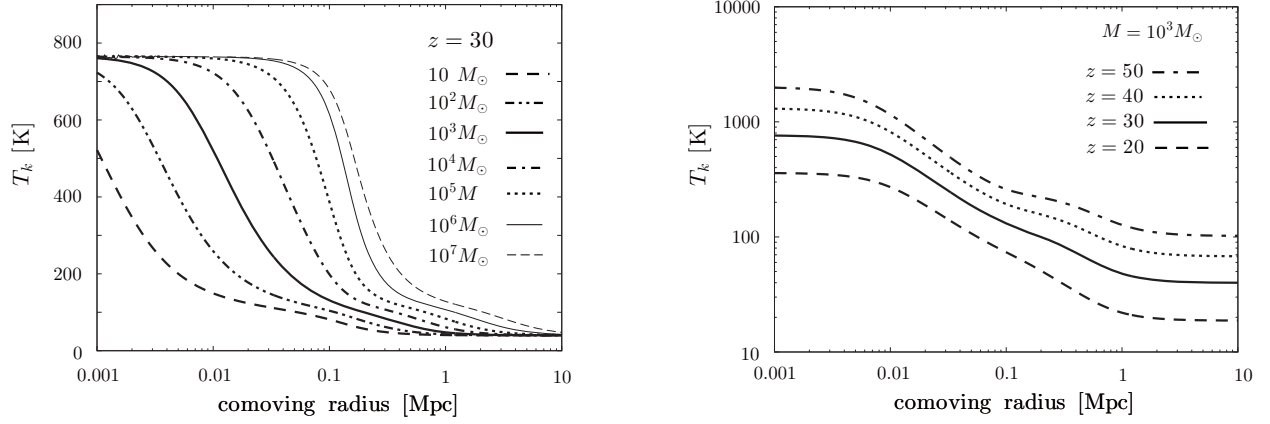


Figure 2. The kinetic temperature of hydrogen gas as a function of the comoving radius. The left panel shows the dependence on PBH mass at $z = 30$. The right panel shows the dependence on the redshift for a PBH with $M = 10^3 M_\odot$. In both panels, the representations of lines are same as in Fig. 1.

recombination term, we can write the evolution of the neutral fraction as

$$\frac{dx_H}{dt} = -\Gamma x_H. \quad (9)$$

The solution of this equation is roughly $x_H \approx \exp(-\Gamma/H)$. Although the radial distance where x_H reaches 0.8 is same as in the case of the ionization-recombination equilibrium, the resultant ionization profile has a sharper edge. This is because most of the ionization photons are absorbed to ionize the inner region. Accordingly, there are not enough ionization photons to ionize the outer region. This fact also means that the heating efficiency is suppressed as the radial distance increases, compared with the case of the ionization-recombination equilibrium. As a result, the heated region becomes one-fifth times smaller than in the previous case.

3 21 CM BRIGHTNESS TEMPERATURE DUE TO A PBH

As shown in the previous section, a PBH ionizes and heats the surrounding region by the X-ray emissions. These ionization and heating leave an observable signature as the differential brightness temperature of the 21 cm intensity relative to the CMB temperature.

The 21 cm intensity depends on the ratio between the number density of neutral hydrogen in the excited state and in the ground state of the hyperfine structure. This ratio can be quantified by the spin temperature T_s . The spin temperature is determined by the balance between three processes: absorption of CMB photons, collisional excitation in the kinetic temperature T_k , and Lyman α pumping (Wouthuysen 1952; Field 1958). In the steady state approximation between these processes, the spin temperature is obtained by (Field 1958)

$$T_s = \frac{T_* + T_\gamma + y_k T_k + y_\alpha T_k}{1 + y_k + y_\alpha}, \quad (10)$$

where T_* is 0.068 K which is the temperature corresponding to the energy difference between the levels in the hyperfine structure, and y_k and y_α are the kinetic and Lyman- α coupling efficiencies, respectively. The kinetic efficiency is given by

$$y_k = \frac{T_*}{A_{10} T_k} (C_H + C_e + C_p), \quad (11)$$

where A_{10} is the Einstein spontaneous emission rate coefficient, $A_{10} = 2.9 \times 10^{-15} \text{ s}^{-1}$. The terms, C_H , C_e and C_p , represent the de-excitation rates due to neutral hydrogen, electrons and protons, respectively. Here we use the fitting formula by Kuhlen et al. (2006),

$$C_H = n_H \kappa, \quad C_e = n_e \gamma_e, \quad C_p = 3.2 n_p \kappa, \quad (12)$$

where n_e and n_p are the electron and proton number densities, respectively. In Eq. (12), κ is the effective single-atom rate coefficient,

$$\kappa = 3.1 \times 10^{-11} n_H T_k^{0.357} \exp(-32/T_k) \text{ cm}^3 \text{ s}^{-1}, \quad (13)$$

and γ_e is given by $\log(\gamma_e/1 \text{ cm}^3 \text{ s}^{-1}) = -9.607 + 0.5 \log T_k \times \exp(-(\log T_k)^{4.5}/1800)$ for $T_k < 10^4$ K and $\gamma_e = \gamma_e(T_k = 10^4 \text{ K})$ for $T_k > 10^4$ K.

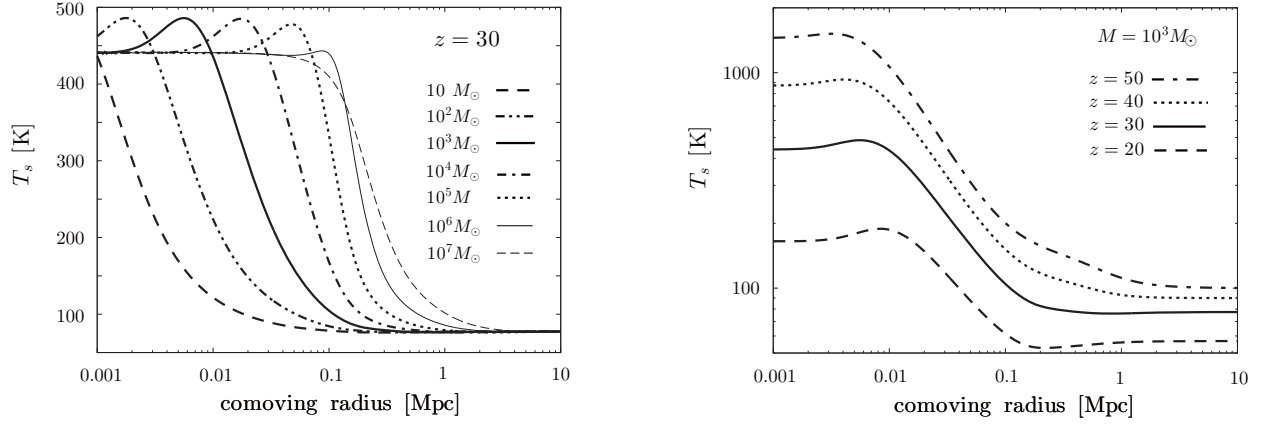


Figure 3. The spin temperature as a function of the comoving radius. The left panel shows the dependence on PBH mass at $z = 30$. The right panel shows the dependence on the redshift for a PBH with $M = 10^3 M_\odot$. In both panels, the representations of lines are same as in Fig. 1.

The Lyman- α coupling efficiency is given by Field (1958),

$$y_\alpha = \frac{16\pi^2 T_* e^2 f_{12} J_0}{27 A_{10} T_k m_e c}, \quad (14)$$

where $f_{12} = 0.416$ is the oscillator strength of the Lyman α transition, and e and m_e are the electron charge and mass, respectively. In Eq. (14), J_0 is the flux of the Lyman α photons due to collisional excitations. At the distance r from the source, J_0 can be written as (Zaroubi et al. 2007)

$$J_0(r) = \frac{\phi_\alpha c}{4\pi H(z) \nu_\alpha} n_H x_H(r) \int_{E_0}^{\infty} \sigma(E) \mathcal{N}(E; r) \frac{dE}{h\nu_\alpha}, \quad (15)$$

where ϕ_α is the fraction of the absorbed energy going into the collisional excitation of Lyman α . Shull & van Steenberg (1985) gave the following analytical form,

$$\phi_\alpha \approx 0.48 (1 - (1 - x_H)^{0.27})^{1.52}. \quad (16)$$

Now we can calculate the spin temperature for a PBH according to the results in the previous section. We show the results in Fig. 3. The left panel shows the spin temperature for different masses of a PBH at $z = 30$ and the right panel represents the spin temperature for different redshifts for $M = 10^3 M_\odot$.

In the highly ionized region, the profile of the spin temperature is flat and does not depend on the PBH mass as shown in the left panel of Fig. 3. Because the PBH can ionize surrounding gas, the spin temperature is determined by the CMB temperature and the term of the kinetic efficiency. As the neutral fraction goes up with increasing distance, however, the Lyman α efficiency y_α becomes larger so that the Lyman α coupling begins to be effective. The peaks of T_s at small radius for small PBH masses shown in the left panel are caused due to this effect. It should note that the peak values are also independent of mass since T_s approaches T_k for a large value of y_α . Because the flux of Lyman- α quickly decreases as the radius increases, the spin temperature also drops. Finally, the spin temperature settles down to the one determined by the background CMB and kinetic temperatures. The larger the PBH mass is, the larger the region where the spin temperature is higher than the background one becomes.

Because the kinetic temperature strongly depends on the redshift as shown in the right panel of Fig. 2, the amplitude of the spin temperature also has strong dependence on the redshift as shown in the right panel of Fig. 3. The spin temperature is almost same as the kinetic temperature in the ionized region at high redshifts ($z > 40$), since the kinetic efficiency y_k dominates other contributions in Eq. (10). In low redshifts ($z < 30$), we find the region where the spin temperature is lower than the background one at the edge of the heated region. In these redshifts the background spin temperature is almost the CMB temperature, while the background spin temperature is between the CMB and kinetic temperatures in redshifts, $30 < z < 50$. Since the kinetic temperature is lower than the CMB temperature at the edge, the Lyman- α coupling is strong and draws the spin temperature toward the kinetic temperature. Therefore, there exists a region where the spin temperature becomes lower than the background one. This tendency appears even in Zaroubi et al. (2007).

The differential brightness temperature from the CMB temperature for a given spin temperature T_s is obtained by (Ciardi & Madau 2003)

$$\delta T_b = (20 \text{ mK}) (1 + \delta) \left(\frac{x_H}{h} \right) \left(1 - \frac{T_\gamma}{T_s} \right) \left(\frac{\Omega_B h^2}{0.0223} \right) \left[\left(\frac{1+z}{10} \right) \left(\frac{0.24}{\Omega_M} \right) \right]^{1/2}, \quad (17)$$

where δ is the density contrast. Here we assume $\delta = 0$ as mentioned in section 2. In Fig. 4, δT_b is shown as a function of the comoving radial distance from a PBH. The left panel is for different masses of a PBH at $z = 30$ and the right panel is

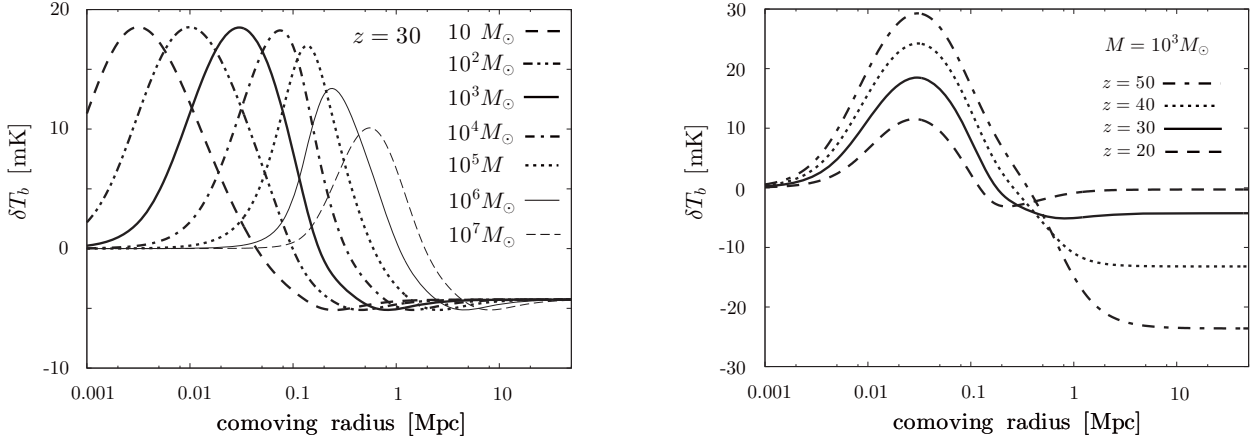


Figure 4. The brightness temperature fluctuations as a function of the comoving radius. The left panel shows the dependence on PBH mass at $z = 30$. The right panel shows the dependence on the redshift for a PBH with $M = 10^3 M_\odot$. In both panels, the representations of lines are same as in Fig. 1.

for different redshifts for $M = 10^3 M_\odot$. The δT_b is almost zero near the source, because hydrogen in such regions are totally ionized. As the neutral fraction increases, the brightness temperature also grows. The peak amplitudes of δT_b are independent on the PBH mass for $M < 10^4 M_\odot$. This is because the spin temperature is much larger than the CMB temperature, $T_s \gg T_\gamma$. Accordingly, from Eq. (17), δT_b becomes independent on T_s and only depends on $(1+z)^{1/2}$. This redshift dependence is shown in the right panel of Fig. 4. On the other hand, the peak amplitude becomes smaller for a mass of the PBH higher than $10^5 M_\odot$ in our model.

As in the case of T_s , the region where the differential brightness temperature is below the background value exists near the edge at $z < 30$. Eventually, however, δT_b matches the background value at a large distance. The size of the region where we can detect δT_b becomes larger with increasing mass, and reaches almost 10 Mpc .

4 THE ANGULAR POWER SPECTRUM OF 21 CM BRIGHTNESS TEMPERATURE DUE TO PBHS

In order to study the potential of cosmological 21 cm observations to give a constraint on the PBH abundance, we evaluate the angular power spectrum of 21 cm fluctuations due to PBHs with mass M .

The observed δT_{obs} at the direction $\hat{\mathbf{n}}$ is the contribution from the IGM along the line of sight. We can obtain δT_{obs} at the observation frequency ν by the integration over the comoving distance r .

$$\delta T_{\text{obs}}(\hat{\mathbf{n}}, \nu) = \int dr W(r, \nu) \delta T_b(r \hat{\mathbf{n}}) \quad (18)$$

where $W(r, \nu)$ is the window function of a 21 cm observation with the frequency ν and $\delta T_b(\mathbf{x})$ is the differential brightness temperature at the position \mathbf{x} , which is produced by PBHs with mass M .

In order to calculate the angular power spectrum, we employ the flat sky approximation and the Limber approximation, since we are only interested in the brightness temperature fluctuations on small scales ($\ell \gg 10$). In these approximation, the angular power spectrum can be written in terms of the three dimensional power spectrum of the brightness temperature (Dodelson 2003),

$$C_\ell(z_{\text{obs}}) = \int dr \frac{W^2(r, \nu)}{r^2} P(k, r), \quad (19)$$

where z_{obs} is the redshift by choosing the observation frequency $\nu = (1 + z_{\text{obs}})\nu_{21}$ with $\nu_{21} = 1420$. MHz, and $P(k, r)$ is the power spectrum of the brightness temperature fluctuations due to PBH with mass M at r .

We obtain the power spectrum of the brightness temperature fluctuations $P(k, r)$, following the halo formalism (Seljak 2000). The power spectrum $P(k, r)$ can be divided to two contributions; the Poisson contribution and clustering contribution. On large scales, since PBHs may be biased tracers of the linear matter power spectrum, they can make the clustering contribution. However, there is theoretical uncertainty in PBH bias. To avoid such uncertainty, we focus on only the Poisson contribution. Therefore, the power spectrum due to PBHs is expressed by

$$P(k, r) = n_{\text{PBH}}(M) |\Delta T_b^2(k)|^2, \quad (20)$$

where $n_{\text{PBH}}(M)$ is the comoving number density of PBHs with M .

The comoving number density of PBHs is described by using the density parameter Ω_{PBH} as

$$n_{\text{PBH}}(M) = \frac{\rho_c \Omega_{\text{PBH}}}{M} = 1.36 \times 10^{-2} \left(\frac{\Omega_{\text{PBH}}}{10^{-9}} \right) \left(\frac{M}{10^4 M_\odot} \right)^{-1} \text{ Mpc}^{-3}, \quad (21)$$

where ρ_c is the critical density at the present epoch. In Eq. (20), $\Delta T_b(k)$ is the Fourier transform of the brightness temperature fluctuations from the background value,

$$\Delta T_b(k) = 4\pi \int x^2 dx (\delta T_b(x) - \delta T_{b0}) \frac{\sin(xk)}{xk}, \quad (22)$$

where $\delta T_b(x)$ is the differential brightness temperature at the comoving radius x from a PBH and δT_{b0} is the background brightness temperature given by Eqs. (10) and (17) with the background kinetic temperature, T_{k0} .

Using $\delta T_b(x)$ obtained in the previous section as shown in Fig. 4, we calculate the angular power spectrum. The results are shown in Fig. 5. Here we set $\Omega_{\text{PBH}} = 10^{-11}$. For simplicity, we assume that the window function has a strong peak at $r = r_{\text{obs}}$ where r_{obs} corresponds to the comoving radial distance at z_{obs} . We approximate the window function as $W^2(r, r_{\text{obs}}) = \delta(r - r_{\text{obs}})$. Since the promising signal of the cosmological 21 cm fluctuations is one due to the primordial density fluctuations, we also plot the angular power spectrum of those fluctuations obtained through CAMB (Lewis & Challinor 2007).

In the left panel of Fig. 5, it is shown that the peak amplitude of the angular spectrum is independent on PBH's mass. The peak locations shift toward large scales for massive PBHs. Moreover, the power law index of the spectrum matches the one due to the primordial density fluctuations on small ℓ 's. The overall amplitude of the spectrum is simply proportional to Ω_{PBH} or the PBH number density. For $\Omega_{\text{PBH}} = 10^{-11}$, it is shown that the angular spectrum of PBHs with mass $10^3 M_\odot$ matches with the one due to the primordial density fluctuations at $z = 30$. It is clear that the spectrum with heavier (lighter) PBHs becomes comparable with primordial density fluctuations' one if Ω_{PBH} is smaller (larger). To match these two spectra, we find the critical value of Ω_{PBH} as $\Omega_{\text{PBHc}} \equiv 10^{-11} (M/10^3 M_\odot)^{-0.2}$ for $z = 30$. The PBH spectrum dominates over the one due to the primordial density fluctuations if Ω_{PBH} exceeds Ω_{PBHc} .

The right panel of Fig. 5 shows that, although the peak location does not depend on the redshift, the redshift dependence of the peak amplitude is different from that due to the primordial density fluctuations.

As the result, while the PBH contribution for Ω_{PBHc} is subdominant at $z = 40$, even the PBHs with roughly $0.1 \times \Omega_{\text{PBHc}}$ can produce the spectrum comparable with that due to the primordial density fluctuations at $z = 20$.

The brightness temperature profile at lower redshifts, $z < 30$, has both positive and negative peaks as shown in Fig. 4. The reason to have a negative peak is because there exists a region where the brightness temperature is lower than the background, which is rather difficult to see in the figure. Accordingly, the angular power spectrum due to PBHs also has two peaks at $z < 30$ as shown in Fig. 5. The peak on a larger scale is due to the negative peak of ΔT_b , while that on a smaller scale is caused by the positive one.

At the last of this section, we discuss the constraint by a future observation such as the square kilometer array (SKA)-like interferometer. Measuring 21 cm anisotropies at high redshifts is a major challenge. The sky at corresponding frequencies is contaminated by foreground due to synchrotron emissions from the Galaxy and extragalactic sources. The noise power spectrum of an observation including the beam effects is given by (Knox 1995)

$$\frac{\ell(\ell+1)}{2\pi} N_\ell^{21} = \frac{\ell(\ell+1)}{t_{\text{obs}} \Delta\nu} \left(\frac{D \lambda T_{\text{sys}}}{A_{\text{eff}}} \right)^2 \exp \left[\frac{\ell(\ell+1)}{\ell_b^2} \right], \quad (23)$$

where A_{eff} is the effective area T_{sys} is the system temperature, t_{obs} is the observation time, $\Delta\nu$ is the frequency bandwidth, D is the length of the baseline and ℓ_b is given by $\ell_b = 4\sqrt{\ln 2}/\theta_{f_w}$ with the resolution $\theta_{f_w} \sim \lambda/D$. Here we adopt the current design of SKA¹; $A_{\text{eff}} = 1 \text{ km}^2$, $t_{\text{obs}} = 1000 \text{ hour}$, $\Delta\nu = 0.1 \text{ MHz}$ and $D = 5 \text{ km}$. We set the system temperature to the sky temperature in minimum emission regions at high Galactic latitudes given by $T_{\text{sys}} = 180(\nu/180 \text{ MHz})^{-2.6} \text{ K}$. In this design, the noise power spectrum is evaluated as

$$\frac{\ell(\ell+1)}{2\pi} N_\ell^{21} \sim 0.9 \times 10^5 \text{ mK}^2 \left(\frac{\ell}{1000} \right)^2 \left(\frac{1+z}{30} \right)^{7.2} \exp \left[\left(\frac{\ell}{2500} \frac{z+1}{30} \right)^2 \right]. \quad (24)$$

The noise power spectrum exponentially grows on larger multipoles than $\ell_b = 2500(30/(1+z))$. The amplitude of the angular power spectrum due to the PBHs is scaled by Ω_{PBH} . Accordingly we find that, in order to dominate over the noise spectrum, $\Omega_{\text{PBH}} \sim 10^{-5} (M/10^3 M_\odot)^{-0.2}$ is required for $M > 10 M_\odot$ at $z = 30$ and $\Omega_{\text{PBH}} \sim 10^{-7} (M/10^3 M_\odot)^{-0.2}$ is for $M > 10 M_\odot$ at $z = 20$. Since the angular spectrum due to PBHs with mass less than $10 M_\odot$ has a peak on larger multipoles than ℓ_b in the SKA design, there is no opportunity to measure the anisotropy spectrum due to such small mass PBHs by SKA.

¹ <http://www.skatelescope.org/>

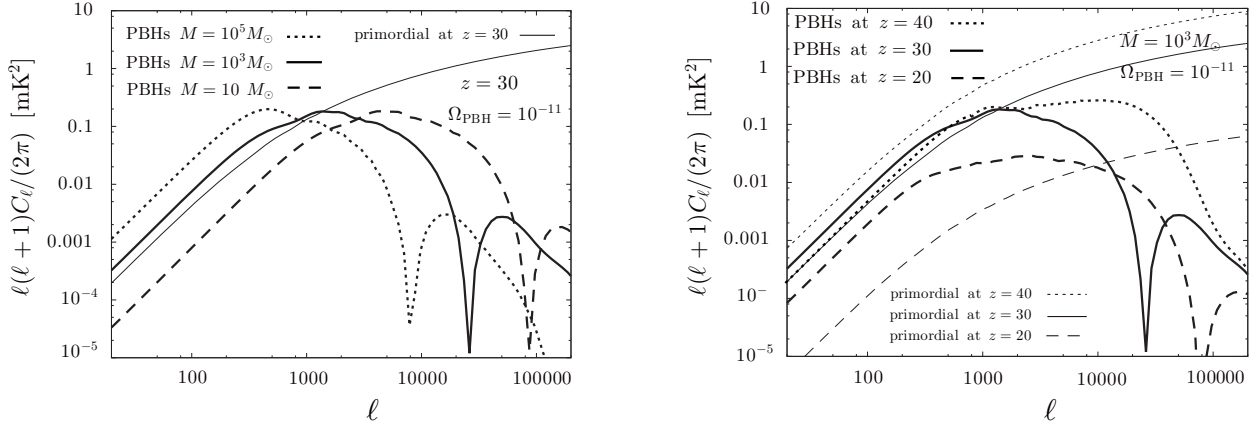


Figure 5. The angular power spectrum of 21 cm brightness temperature fluctuations produced by PBHs as the function of comoving radius. The left panel shows the dependence on the PBH mass at $z = 30$. The dotted, solid and dashed lines represent for PBHs with $M = 10^5 M_\odot$, $10^3 M_\odot$ and $10 M_\odot$, respectively. The right panel shows the dependence on the redshift for PBHs with $M = 10^3 M_\odot$. The dotted, solid and dashed lines are for PBHs at $z = 40$, $z = 30$ and $z = 20$, respectively. We assume $\Omega_{\text{PBH}} = 10^{-11}$ in both panels. For comparison, we also plot the angular power spectrum due to the primordial density fluctuations as thin lines.

5 CONCLUSION

We have investigated the 21 cm signal produced by massive PBHs whose masses are larger than $10 M_\odot$. Assuming a power-law spectrum of X-ray photons from an accretion disk, we have studied the ionization and heating of IGM gas near a PBH and evaluated the differential 21 cm brightness temperature. We have shown that a PBH can induce an observable signal of differential 21 cm brightness temperature. The size of the region where we can find the differential brightness temperature typically reaches 1–10 Mpc for our interested PBH mass range. The exact size depends on the PBH mass.

We have also calculated the angular power spectrum of 21 cm fluctuations due to PBHs. The peak position of the angular spectrum depends on the PBH mass, while the amplitude is independent of the mass. Comparing this spectrum with the angular power spectrum caused by primordial density fluctuations, we have found that both of them become comparable if $\Omega_{\text{PBH}} = 10^{-11} (M/10^3 M_\odot)^{-0.2}$ at $z = 30$ and $10^{-12} (M/10^3 M_\odot)^{-0.2}$ at $z = 20$ for PBH’s mass from $10 M_\odot$ to $10^8 M_\odot$. If the density parameter is larger than these values, the angular power spectrum due to PBHs exceeds the one from primordial fluctuations and can be measured. In other words, we cannot set constraints on the PBH density parameter below these values from 21 cm observations. If we consider the sensitivity of the SKA-like observation, for example, we can detect the signal of PBHs up to $\Omega_{\text{PBH}} = 10^{-5} (M/10^3 M_\odot)^{-0.2}$ at $z = 30$ and $10^{-7} (M/10^3 M_\odot)^{-0.2}$ at $z = 20$ for PBHs with mass from $10^2 M_\odot$ to $10^8 M_\odot$.

The ionization of IGM due to PBHs with such density parameters does not affect the global reionization history of the universe since reionization from each PBH only covers a tiny patch of the universe. Unlike reionization from first stars, therefore, such reionization has little impact on CMB temperature anisotropies. On the other hand, PBHs can heat IGM regions whose scale reaches 1-10Mpc and 21 cm fluctuations are sensitive to the heated IGM regions. Accordingly the PBH density parameter constrained from WMAP data, that is $\Omega_{\text{PBH}} < 10^{-7}$ (Ricotti et al. 2008), is several order of magnitude larger than the values at which 21 cm fluctuations from PBHs comparable with those from primordial density fluctuations as we mentioned above. In other words, we can conclude that, if observation instruments or foreground removal are more improved than the current SKA design, 21 cm fluctuation observations have a potential to probe the PBH abundance which is impossible to access by CMB observations.

The most theoretical uncertainty in this model is the flux of photons due to the accretion to PBHs. In this paper, we assume that the X-ray photon flux amplitude is a tenth of the Eddington luminosity and has the power law spectrum with E^{-1} for simplicity. We also studied the effect of the power law index by changing to $E^{-1/2}$. The temperature profile shifts to a smaller scale due to the decrease of the ionization efficiency. However this shift is small, and the resultant angular power spectrum does not change much.

The amplitude of the luminosity is considered to depend on the matter accretion rate onto a PBH. Ricotti et al. (2008) have studied the luminosity for the Bondi-Hoyle accretion in detail. Although the luminosity depends on the PBH mass and feedback effect on the ionization and temperature, they have shown that the luminosity for a PBH with $M = 10^3 M_\odot$ is roughly a hundredth of the Eddington luminosity at $z > 20$. In our model, the brightness temperature profile near a PBH at a certain redshift depends only on the PBH’s mass and the amplitude of the angular power spectrum is scaled by Ω_{PBH} . Therefore, if we assume that the amplitude of the X-ray photon flux is a hundredth of the Eddington luminosity, the required density parameter for PBHs to dominate the 21 cm fluctuations due to primordial density fluctuations is $10^{-11} (M/10^4 M_\odot)^{-0.2}$ at $z = 30$ and $10^{-12} (M/10^4 M_\odot)^{-0.2}$ at $z = 20$ for PBH’s mass from $10 M_\odot$ to $10^8 M_\odot$.

ACKNOWLEDGMENTS

We thank A. Long for useful comments. H. T. is supported by the DOE at Arizona state university. N. S. is supported by Grand-in-Aid for Scientific Research No. 22340056. This research has also been supported in part by World Premier International Research Center Initiative, MEXT, Japan.

REFERENCES

- Alcock C., et al. 2001, *Astrophys. J. Lett.*, 550, L169
 Carr B. J., 1975, *Astrophys. J.*, 201, 1
 Carr B. J., 1981, *MNRAS*, 194, 639
 Carr B. J., Hawking S. W., 1974, *MNRAS*, 168, 399
 Carr B. J., Kohri K., Sendouda Y., Yokoyama J., 2010, *Phys. Rev. D*, 81, 104019
 Ciardi B., Madau P., 2003, *Astrophys. J.*, 596, 1
 Dijkstra M., Haiman Z., Loeb A., 2004, *Astrophys. J.*, 613, 646
 Dodelson S., “Modern cosmology,” Amsterdam, Netherlands: Academic Pr. (2003) 440 p
 DÜchting N., 2004, *Phys. Rev. D*, 70, 064015
 Field G. B., 1958, *Proc. IRE*, 46, 240
 Gnedin N. Y., Ostriker J. P., Rees M. J., 1995, *Astrophys. J.*, 438, 40
 Green A. M., Liddle A. R., Malik K. A., Sasaki M., 2004, *Phys. Rev. D*, 70, 041502
 Hawking S. W., 1974, *Nature*, 248, 30
 Inoue K. T., Tanaka T., 2003, *Physical Review Letters*, 91, 021101
 Ioka K., Tanaka T., Nakamura T., 1999, *Phys. Rev. D*, 60, 083512
 Khlopov M. Y., Rubin S. G., Sakharov A. S., 2005, *Astroparticle Physics*, 23, 265
 Knox L., 1995, *Phys. Rev. D*, 52, 4307
 Komatsu E., et al. 2011, *Astrophys. J. Suppl.*, 192, 18
 Kuhlen M., Madau P., 2005, *MNRAS*, 363, 1069
 Kuhlen M., Madau P., Montgomery R., 2006, *Astrophys. J. Lett.*, 637, L1
 Lewis A., Challinor A., 2007, *Phys. Rev. D*, 76, 083005
 Lindley D., 1980, *MNRAS*, 193, 593
 MacGibbon J. H., Carr B. J., 1991, *Astrophys. J.*, 371, 447
 Mack K. J., Wesley D. H., 2008, arXiv:0805.1531
 Miller M. C., Ostriker E. C., 2001, *Astrophys. J.*, 561, 496
 Miyama S., Sato K., 1978, *Progress of Theoretical Physics*, 59, 1012
 Page D. N., Hawking S. W., 1976, *Astrophys. J.*, 206, 1
 Ricotti M., Ostriker J. P., Mack K. J., 2008, *Astrophys. J.*, 680, 829
 Seljak U., 2000, *MNRAS*, 318, 203
 Shull J. M., van Steenberg M. E., 1985, *Astrophys. J.*, 298, 268
 Tashiro H., Sugiyama N., 2008, *Phys. Rev. D*, 78, 023004
 Vainer B. V., Dryzhakova O. V., Naselskii P. D., 1978, *Soviet Astronomy Letters*, 4, 185 [1978, *Pis ma Astronomicheskii Zhurnal*, 4, 344]
 Vainer B. V., Naselskii P. D., 1978, *Soviet Astronomy*, 22, 138 [1978, *Astronomicheskii Zhurnal*, 55, 231]
 Wouthuysen S. A., 1952, *Astronomical Journal*, 57, 31
 Zaroubi S., Thomas R. M., Sugiyama N., Silk J., 2007, *MNRAS*, 375, 1269
 Zdziarski A. A., Svensson R., 1989, *Astrophys. J.*, 344, 551
 Zeldovich I. B., Starobinskii A. A., Khlopov M. I., Chechetkin V. M., 1977, *Soviet Astronomy Letters*, 3, 110 [1977, *Pis ma Astronomicheskii Zhurnal*, 3, 208]
 Zel’dovich Y. B., Starobinskii A. A., 1976, *Soviet Journal of Experimental and Theoretical Physics Letters*, 24, 571 [1976, *ZhETF Pis ma Redaktsiiu*, 24, 616]